Physics Letters B 761 (2016) 444–449

Contents lists available at ScienceDirect

Physics Letters B

www.elsevier.com/locate/physletb

# On the zero crossing of the three-gluon vertex

A. Athenodorou [a], D. Binosi [b,*], Ph. Boucaud [c], F. De Soto [d], J. Papavassiliou [e], J. Rodríguez-Quintero [f], S. Zafeiropoulos [g]

[a] Department of Physics, University of Cyprus, POB 20537, 1678 Nicosia, Cyprus
[b] European Centre for Theoretical Studies in Nuclear Physics and Related Areas (ECT*) and Fondazione Bruno Kessler, Villa Tambosi, Strada delle Tabarelle 286, I-38050 Villazzano (TN), Italy
[c] Laboratoire de Physique Théorique (UMR8627), CNRS, Univ. Paris-Sud, Université Paris-Saclay, 91405 Orsay, France
[d] Dpto. Sistemas Físicos, Químicos y Naturales, Univ. Pablo de Olavide, 41013 Sevilla, Spain
[e] Department of Theoretical Physics and IFIC, University of Valencia-CSIC, E-46100, Valencia, Spain
[f] Department of Integrated Sciences, University of Huelva, E-21071 Huelva, Spain
[g] Institut für Theoretische Physik, Goethe-Universität Frankfurt, Max-von-Laue-Str. 1, 60438 Frankfurt am Main, Germany

ARTICLE INFO

*Article history:*
Received 7 July 2016
Received in revised form 23 August 2016
Accepted 31 August 2016
Available online 6 September 2016
Editor: J.-P. Blaizot

*Keywords:*
Lattice simulations
Three-gluon vertex
Zero crossing
Schwinger–Dyson equations

ABSTRACT

We report on new results on the infrared behavior of the three-gluon vertex in quenched Quantum Chromodynamics, obtained from large-volume lattice simulations. The main focus of our study is the appearance of the characteristic infrared feature known as 'zero crossing', the origin of which is intimately connected with the nonperturbative masslessness of the Faddeev–Popov ghost. The appearance of this effect is clearly visible in one of the two kinematic configurations analyzed, and its theoretical origin is discussed in the framework of Schwinger–Dyson equations. The effective coupling in the momentum subtraction scheme that corresponds to the three-gluon vertex is constructed, revealing the vanishing of the effective interaction at the exact location of the zero crossing.

© 2016 The Authors. Published by Elsevier B.V. This is an open access article under the CC BY license (http://creativecommons.org/licenses/by/4.0/). Funded by SCOAP[3].

## 1. Introduction

One notable aspect of the ongoing intense exploration of the infrared (IR) sector of Quantum Chromodynamics (QCD) has been the detailed scrutiny of the fundamental Green's functions of the theory using large-volume lattice simulations [1–8], together with a variety of continuum approaches [9–30]. Even though off-shell Green's functions are not physical quantities, given their explicit dependence on the gauge-fixing parameter and the renormalization scheme, they encode valuable information on fundamental nonperturbative phenomena such as confinement, chiral symmetry breaking, and dynamical mass generation, and constitute the basic building blocks of symmetry-preserving formalisms that aim at a veracious description of hadron phenomenology [14,31–38].

The most important findings of the aforementioned studies are related with the two-point sector of the theory. Specifically, it is now firmly established that, in the Landau gauge, the gluon propagator, $\Delta(q^2)$, reaches a finite value in the deep IR, whilst the ghost propagator, $D(q^2)$ remains massless, but with an IR finite dressing function, $F(q^2)$ [note that $D(q^2) = F(q^2)/q^2$]. This characteristic behavior has led to the critical reassessment of previously established theoretical viewpoints, and has sparked a systematic effort towards a 'top-down' derivation of the ingredients that enter in the dynamical equations describing the properties of mesons [38].

The aforementioned results have been interpreted by employing a variety of distinct formalisms, such as the refined Gribov–Zwanziger scenario [22,23], or differently truncated versions of the Schwinger–Dyson equations (SDEs) of the theory [11,13]. One particular approach within this latter framework [39] advocates that (**a**) the gluon acquires dynamically an effective mass [40], through a subtle realization of the Schwinger mechanism, and (**b**) the ghost is transparent to this mechanism, and remains massless; however, its dressing function is protected by the gluon mass, that tames any possible IR divergence and enforces its finiteness at the origin.

This profound difference in the IR behavior between gluons and ghosts induces characteristic effects to other Green's functions [but also to $\Delta(q^2)$], essentially due to the inequivalence between loops containing 'massive' gluons or massless ghosts [41,42]. Specifically, while the former are 'protected' by the gluon mass, $m$, yielding IR finite contributions of the type $\log(q^2 + m^2)$, the latter are

* Corresponding author.
*E-mail address:* binosi@ectstar.eu (D. Binosi).

http://dx.doi.org/10.1016/j.physletb.2016.08.065
0370-2693/© 2016 The Authors. Published by Elsevier B.V. This is an open access article under the CC BY license (http://creativecommons.org/licenses/by/4.0/). Funded by SCOAP[3].

'unprotected', yielding (potentially) IR divergent terms of the type $\log q^2$.

In the case of $\Delta^{-1}(q^2)$, the ghost-loop contained in its self-energy generates a term $q^2 \log q^2$, and therefore remains IR finite; however, the first derivative of $\Delta^{-1}(q^2)$ diverges at the origin, precisely as an unprotected logarithm.

The corresponding effect on the three-gluon vertex is particularly striking. Specifically, in certain special kinematic limits, some of the vertex form factors are dominated in the IR by the corresponding ghost-loop diagram, the leading contribution of which, by virtue of the Slavnov–Taylor identity (STI), turns out to be proportional to the derivative of $\Delta^{-1}(q^2)$. Thus, the form factors reverse sign for sufficiently small momenta, displaying finally a logarithmic divergence at the origin. The transition from positive values (at intermediate and large momenta) to a negative divergence at the origin is associated with the so-called *'zero crossing'*: at some finite energy scale, in the deep IR, the form factors in question vanish. The weak nature of the divergence makes the effect difficult to observe in lattice simulations. Indeed, SU(2) studies [1,2] found the expected pattern in three space–time dimensions (where the IR divergence behaves as $1/q$), but were less conclusive in four dimensions.

We emphasize that independent analyses within the SDE formalism, employing a variety of techniques and truncation schemes, have confirmed these claims in the three-point [43–46] and the four-point [47,48] gluon sector. In addition, unquenching techniques, such as those developed in [49,50], coupled with the lattice results of [7], show that the presence of light quarks slightly modifies the behavior of the gluon and ghost two-point sector only at the quantitative level; therefore, the expected IR pattern 'zero crossing plus logarithmic IR divergence' for $n$-point gluon Green's functions seems to constitute a robust prediction *for QCD*.[1]

In this letter, we present new results for the three-gluon vertex obtained from SU(3) lattice simulations in large four-dimensional volumes. We restrict our analysis to the tensorial structure corresponding to that of the three-gluon vertex, which is obtained as a particular projection of the full lattice three-point function, after the amputation of the external gluon legs. The results strongly support the appearance of a zero crossing in the case of one of the two kinematic configurations considered ('symmetric' configuration). On the other hand, in the case of the second kinematic choice ('asymmetric' configuration), the presence of a zero crossing cannot be clearly discerned. The theoretical origin of this special feature is reviewed within the framework of the SDEs, and the three-gluon running coupling, defined in the momentum subtraction (MOM) scheme, numerically extracted from the data. Finally, the limitations of the semiclassical approach in accounting for the observed behavior of the three-gluon vertex in the IR are briefly discussed.

## 2. Three-gluon vertex, renormalization, and effective charge

The connected three-gluon vertex is defined as the correlation function[2] ($q+r+p=0$)

$$\mathcal{G}^{abc}_{\alpha\mu\nu}(q,r,p) = \langle A^a_\alpha(q) A^b_\mu(r) A^c_\nu(p)\rangle = f^{abc}\mathcal{G}_{\alpha\mu\nu}(q,r,p), \tag{1}$$

where $A$ denotes the gauge field with sub (super) indices representing Lorentz (color) indices, and the average $\langle\cdot\rangle$ indicates functional integration over the gauge space. In terms of the usual 1-particle irreducible (1-PI) function, one has

$$\mathcal{G}_{\alpha\mu\nu}(q,r,p) = g\Gamma_{\alpha'\mu'\nu'}(q,r,p)\Delta_{\alpha'\alpha}(q)\Delta_{\mu'\mu}(r)\Delta_{\nu'\nu}(p), \tag{2}$$

with $g$ the strong coupling constant. In the Landau gauge, the transversality of the gluon propagator, *viz.*,

$$\Delta^{ab}_{\mu\nu}(q) = \langle A^a_\mu(q) A^b_\nu(-q)\rangle = \delta^{ab}\Delta(p^2)P_{\mu\nu}(q), \tag{3}$$

where $P_{\mu\nu}(q) = \delta_{\mu\nu} - q_\mu q_\nu/q^2$, implies directly that $\mathcal{G}$ is totally transverse: $q\cdot\mathcal{G} = r\cdot\mathcal{G} = p\cdot\mathcal{G} = 0$.

There are only four totally transverse tensor structures that can be constructed out of three Lorentz indices and two linearly independent four-vectors, which are also compatible with the required Bose symmetry of the vertex [53]. One of them can be always taken to be proportional to the tree-level form

$$\lambda^{\rm tree}_{\alpha\mu\nu}(q,r,p) = \Gamma^{(0)}_{\alpha'\mu'\nu'}(q,r,p)P_{\alpha'\alpha}(q)P_{\mu'\mu}(r)P_{\nu'\nu}(p). \tag{4}$$

The remaining tensors will be then chosen depending on which of the two special momenta configurations, studied in the ensuing analysis, will be considered.

The first configuration will be the so-called *symmetric* configuration, in which $q^2 = r^2 = p^2$ and $q\cdot r = q\cdot p = r\cdot p = -q^2/2$; in this case, there is only one possible extra independent tensor, namely [54,55]

$$\lambda^{S}_{\alpha\mu\nu}(q,r,p) = (r-p)_\alpha(p-q)_\mu(q-r)_\nu/r^2. \tag{5}$$

Then, indicating with $S^{\rm sym}$ and $T^{\rm sym}$ (respectively, $\Gamma^{\rm sym}_S$ and $\Gamma^{\rm sym}_T$) the corresponding form factors in the decomposition of $\mathcal{G}$ (respectively, $\Gamma$) in this momentum configuration, Eq. (2) implies the relation

$$\begin{aligned} T^{\rm sym}(q^2) &= g\,\Gamma^{\rm sym}_T(q^2)\,\Delta^3(q^2),\\ S^{\rm sym}(q^2) &= g\,\Gamma^{\rm sym}_S(q^2)\,\Delta^3(q^2). \end{aligned} \tag{6}$$

In particular, the $T^{\rm sym}$ form factor can be projected out through

$$T^{\rm sym}(q^2) = \left.\frac{W^{abc}_{\alpha\mu\nu}(q,r,p)\,\mathcal{G}^{abc}_{\alpha\mu\nu}(q,r,p)}{W^{abc}_{\alpha\mu\nu}(q,r,p)W^{abc}_{\alpha\mu\nu}(q,r,p)}\right|_{\rm sym}, \tag{7}$$

with $W^{abc}_{\alpha\mu\nu} = f^{abc}(\lambda^{\rm tree}_{\alpha\mu\nu} + \lambda^{S}_{\alpha\mu\nu}/2)$.

The second configuration will be the so-called *asymmetric* configuration, which is defined by taking the $q\to 0$ limit, while imposing at the same time the condition $r^2 = p^2 = -p\cdot r$. In this case, no tensor other than the tree-level form can be constructed, with Eq. (4) reducing in this case to [54,55]

$$\lambda^{\rm tree}_{\alpha\mu\nu}(0,r,-r) = 2r_\alpha P_{\mu\nu}(r). \tag{8}$$

Thus, one is left with a single form factor, which can be projected out through

$$\begin{aligned} T^{\rm asym}(r^2) &= \left.\frac{W^{abc}_{\alpha\mu\nu}(q,r,p)\,\mathcal{G}^{abc}_{\alpha\mu\nu}(q,r,p)}{W^{abc}_{\alpha\mu\nu}(q,r,p)W^{abc}_{\alpha\mu\nu}(q,r,p)}\right|_{\rm asym}\\ &= g\,\Gamma^{\rm asym}_T(r^2)\,\Delta(0)\,\Delta^2(r^2), \end{aligned} \tag{9}$$

where now $W^{abc}_{\alpha\mu\nu} = f^{abc}\lambda^{\rm tree}_{\alpha\mu\nu}$.

All the quantities defined so far are bare, and a dependence on the regularization cut-off must be implicitly understood. Within a given renormalization procedure, the renormalized Green's functions are calculated in terms of the renormalized fields $A_R = Z_A^{-1/2}A$, so that

[1] Notice, however, that, at least in the case of the three-gluon vertex, recent theoretical studies [51,52] show that light quarks will shift the zero crossing deeper in the IR, which might render it undetectable in current full QCD lattice simulations.

[2] In general, the SU(3) vertex contains also terms proportional to the completely symmetric group structure $d^{abc}$; however, all such terms will be annihilated upon their contraction with the $f^{abc}$ that multiplies the projectors $W$ entering in Eqs. (7) and (9).

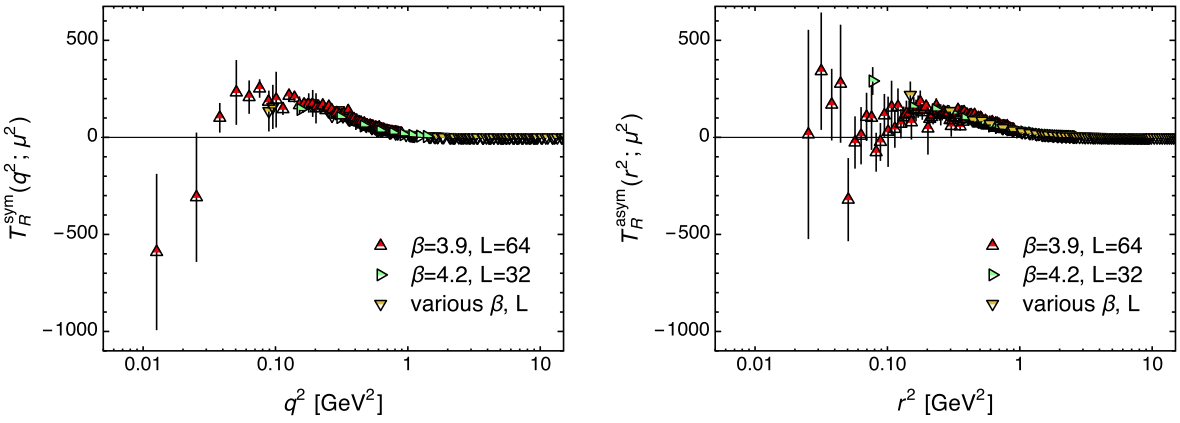


**Fig. 1.** (Color online.) Lattice results for the renormalized connected form factor $T_R$ in the symmetric (left) and asymmetric (right) momentum configuration. For both data sets the renormalization point $\mu = 4.3$ GeV was chosen. The same scale is used in both plots which reveals the similar behavior of the two form factors.

$$\Delta_R(q^2;\mu^2) = Z_A^{-1}(\mu^2)\,\Delta(q^2),$$
$$T_R^{\rm sym}(q^2;\mu^2) = Z_A^{-3/2}(\mu^2) T^{\rm sym}(q^2), \tag{10}$$

and similarly for the asymmetric configuration. Within the MOM scheme that we will employ, one then requires that all the Green's functions take their tree-level expression at the subtraction point, namely

$$\Delta_R(q^2;q^2) = Z_A^{-1}(q^2)\,\Delta(q^2) = 1/q^2,$$
$$T_R^{\rm sym}(q^2;q^2) = Z_A^{-3/2}(q^2)\,T^{\rm sym}(q^2) = g_R^{\rm sym}(q^2)/q^6. \tag{11}$$

The first equation yields the renormalization constant $Z_A$ as a function of the bare propagator, which when substituted into the second equation provides a definition of the $\mu$-independent three-gluon MOM running coupling [54,55]:

$$g^{\rm sym}(q^2) = q^3 \frac{T^{\rm sym}(q^2)}{[\Delta(q^2)]^{3/2}} = q^3 \frac{T_R^{\rm sym}(q^2;\mu^2)}{[\Delta_R(q^2;\mu^2)]^{3/2}}. \tag{12}$$

In the asymmetric configuration the relation is slightly different, as in this case one has

$$T_R^{\rm asym}(r^2;r^2) = Z_A^{-3/2}(r^2)\,T^{\rm asym}(r^2) = \Delta_R(0;q^2)\,g_R^{\rm asym}(r^2)/r^4, \tag{13}$$

implying the $\mu$-independent definition

$$g^{\rm asym}(r^2) = r^3 \frac{T^{\rm asym}(r^2)}{[\Delta(r^2)]^{1/2}\Delta(0)} = r^3 \frac{T_R^{\rm asym}(r^2;\mu^2)}{[\Delta_R(r^2;\mu^2)]^{1/2}\Delta_R(0;\mu^2)}. \tag{14}$$

Finally, in both cases the above equations yield for the 1-PI form factors the relation

$$g^i(\mu^2)\,\Gamma^i_{T,R}(\ell^2;\mu^2) = \frac{g_R^i(\ell^2)}{[\ell^2\Delta(\ell^2;\mu^2)]^{3/2}}, \tag{15}$$

where $i$ indicates either the symmetric or the asymmetric momentum configuration, and, correspondingly, $\ell^2 = q^2$, $r^2$.

This latter result is of special interest because it establishes a connection between the three-gluon MOM running coupling, which many lattice and continuum studies have paid attention to, and the vertex function of the amputated three-gluon Green's function, a fundamental ingredient within the tower of (truncated) SDEs addressing non-perturbative QCD phenomena. In fact, these quantities are related only by the gluon propagator $\Delta$, which, after the intensive studies of the past decade, is very well understood and accurately known.

## 3. Lattice set-up and results

The lattice set-up used for our simulations is that of [56], where quenched SU(3) configurations for different bare couplings $\beta$ and lattice volumes were obtained employing the tree-level Symanzik gauge action. In particular, we use 220 configurations at $\beta = 4.20$ for a hypercubic lattice of length $L = 32$ (physical volume of $4.5^4$ fm$^4$) and 900 configurations at $\beta = 3.90$ and $L = 64$ (physical volume of $15.6^4$ fm$^4$). The data extracted from these new gauge configurations have been supplemented with the one derived from the old configurations of [57], obtained using the Wilson gauge action at several $\beta$ (ranging from 5.6 to 6.0), lattices (from $L = 24$ to 32) and physical volumes (from $2.4^4$ to $5.9^4$ fm$^4$).

In Fig. 1 we plot the form factor $T$ renormalized at $\mu = 4.3$ GeV for both the symmetric (left panel) and asymmetric (right panel) momentum configuration. In the symmetric case $T_R^{\rm sym}$ displays a zero crossing located in the IR region around 0.1–0.2 GeV, after which the data seems to indicate that some sort of divergent behavior manifests itself. In the asymmetric case the situation looks less clear as data are noisier, as a result of forcing one momentum to vanish.

## 4. SDE analysis

As was shown in some of the literature cited above (most notably [41,42]), the *nonperturbative* ghost loop diagram contributing to the SDE of $\Delta(q^2)$ is the source of certain noteworthy effects, the underlying origin of which is the masslessness of the propagators circulating in this particular loop. In the present section we briefly review known results, focusing on the aspect needed for the interpretation of the new lattice results presented here.

Specifically, employing a nonperturbative Ansatz for the gluon–ghost vertex that satisfies the correct STI, the leading IR contribution, denoted by $\Pi_c(q^2)$, is given by [42]

$$\Pi_c(q^2) = \frac{g^2 C_A}{6} q^2 F(q^2) \int_k \frac{F(k^2)}{k^2(k+q)^2}, \tag{16}$$

where $C_A$ is the Casimir eigenvalue in the adjoint representation, and $\int_k \equiv \mu^\epsilon/(2\pi)^d \int {\rm d}^d k$ is the dimensional regularization measure, with $d = 4-\epsilon$ and $\mu$ is the 't Hooft mass; evidently, in the limit $q^2 \to 0$, the above expressions behave like $q^2 \log q^2/\mu^2$. Even though this particular term does not interfere with the finiteness of $\Delta(q^2)$, its presence induces two main effects: (*i*) $\Delta(q^2)$ displays a mild maximum at some relatively low value of $q^2$, and (*ii*) the first derivative of $\Delta^{-1}(q^2)$ diverges logarithmically at $q^2 = 0$. The

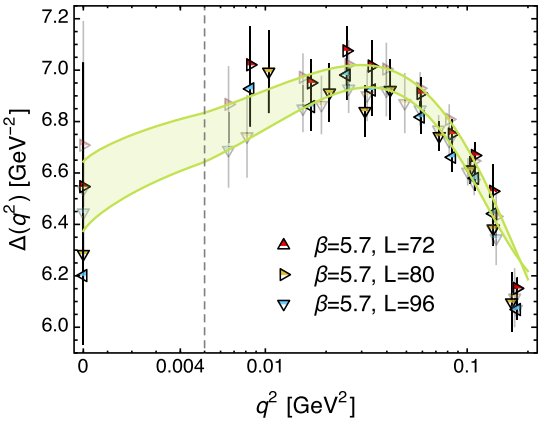


**Fig. 2.** (Color online.) IR fit of the gluon propagator at $\mu = 4.3$ GeV. The actual data fitted, are the semitransparent ones, which are obtained by applying a cubic smooth spline with roughness penalty procedure to the original data [58]. The band indicates the variation of the fit between $L = 72$ and $L = 96$, $L = 80$ being somewhere in between. Notice also that after the dashed vertical line the scale becomes linear, to expose the propagator behavior at the origin.

form of the renormalized gluon propagator that emerges from the complete SDE analysis may be accurately parametrized in the IR by the expression

$$\Delta_R^{-1}(q^2;\mu^2) \underset{q^2\to 0}{=} q^2\left[a + b\log\frac{q^2+m^2}{\mu^2} + c\log\frac{q^2}{\mu^2}\right] + m^2, \tag{17}$$

with $a$, $b$, $c$, and $m^2$ suitable parameters, which captures explicitly the two aforementioned effects. Note that $\Delta_R^{-1}(0;\mu^2) = m^2$, and that the 'protected' logarithms stem from gluonic loops.

Higher order $n$-point functions ($n > 2$) are also affected in notable ways by the presence of ghost loops in their diagrammatic expansion.[3] If the external legs correspond to background gluons (as was the case in [42]), the leading IR behavior of projectors such as (7) and/or (9) is proportional to the derivative of the inverse gluon propagator, by virtue of the Abelian STIs [42]. Thus, eventually, a logarithmic divergence appears, which drives the aforementioned projectors from positive to (infinitely) negative values, causing invariably the appearance of a zero crossing. Use of the 'background quantum' identities [59,60], which relate background Green's functions with quantum ones, reveals that the same behavior is expected for quantum external legs, modulo a (finite) function determined by the ghost–gluon dynamics [42]. The exact position of the zero crossing is difficult to estimate, because it depends on the details of all finite contributions that are 'competing' against the logarithm coming from the ghost loop; however, it is clear that the tendency, in general, is to appear in the deep IR.

In particular, for the form factors under scrutiny, one expects the (configuration independent) IR behavior

$$\Gamma^i_{T,R}(\ell^2;\mu^2) \underset{\ell^2\to 0}{\simeq} F(0;\mu^2)\frac{\partial}{\partial\ell^2}\Delta_R^{-1}(\ell^2;\mu^2), \tag{18}$$

where $F(0) \approx 2.9$ at $\mu = 4.3$ GeV [5].

To see if indeed the lattice data conform to the expected behavior, we start by estimating the propagator's parameters $a$, $b$, $c$ and $m^2$ by fitting the lattice data of [5]. The results are shown in Fig. 2, with the parameter values obtained for the available data sets listed in Table 1. In what follows we will not distinguish between these different fits; rather we will use a single curve with bands representing its 'uncertainty'.

**Table 1**
Best fit parameters for the IR propagator (17) obtained using the SU(3) data of [5] for $\beta = 5.7$ and $L = 72$, 80 and 96 lattices.

| Parameter | $L = 72$ | $L = 80$ | $L = 96$ |
|---|---|---|---|
| $a$ | −0.471 | −0.151 | −1.146 |
| $b$ | −0.546 | −0.458 | −0.922 |
| $c$ | 0.362 | 0.352 | 0.546 |
| $m^2$ | 0.151 | 0.154 | 0.157 |

At this point we can use Eq. (18) and the relation (6) to determine the expected IR behavior of the connected form factors $T^{\rm sym}$ and $T^{\rm asym}$, and compare with the data.[4] The results are shown in Fig. 3. While it is evident that in the symmetric case a good description of the IR data is achieved, in the asymmetric case the positive excess in the data coupled to the large errors make it more difficult to discern the low momentum behavior of $T_R^{\rm asym}$ and $\Gamma_{T,R}^{\rm asym}$.

There is an interesting conclusion one might draw from the behavior of these form factors. As discussed in detail in [56], when quantum fluctuations can be either neglected or suppressed, gluon correlation functions appear to be dominated by a semiclassical background described in terms of a multi-instanton solution. In particular, specializing to the symmetric configuration, one has in this case

$$g^{\rm sym}(\mu^2)\Gamma^{\rm sym}_{T,R}(q^2;\mu^2) \simeq \sqrt{\frac{2}{9np^2\left[\Delta(p^2;\mu^2)\right]^3}}, \tag{19}$$

where $n = 7.7$ fm$^{-4}$ is the instanton density in the semiclassical background. The resulting curve is shown by the dashed line in the lower left panel of Fig. 3. Then, we see that while the approximation (19) appears to be justified for momenta roughly below $q \sim 1$ GeV [56,57], it fails in the deep IR region, around $q \sim 0.2$–$0.3$ GeV. This can be understood once we notice that at such low momenta (where the zero crossing takes place), the dynamics is entirely dominated by massless ghosts; plainly, this is a quantum effect that cannot be captured within the framework of a semiclassical approach.

Next, using Eqs. (12) and (14), we can construct the effective coupling $\alpha^i(\ell^2) = g^{i2}(\ell^2)/4\pi$ both from the lattice data and the determined IR behavior. In particular, the $\alpha^i$ derived from the three-gluon vertex is proportional to the *square* of the form factor $\Gamma_T$, and displays a striking behavior: $\alpha^i$ is forced to vanish at the zero crossing, and then 'bounces' back to positive values, as can be clearly seen in Fig. 4. According to this result, the part of the amplitude 'gluon + gluon → gluon + gluon' that is mediated by the (fully dressed) one-gluon exchange diagram vanishes at some special IR momentum; to be sure, this is not true for the entire physical amplitude, since additional diagrams (such as 'boxes') will furnish nonvanishing contributions.

## 5. Conclusions

We have presented new lattice results for the three-gluon vertex form factor $T$ proportional to the tree-level tensor structure. The data were obtained from large 4-dimensional configurations generated for an SU(3) Yang–Mills theory gauge fixed in the Landau gauge, and the form factor evaluated in the so-called symmetric and asymmetric momentum configurations. The IR behavior

[3] We refer to ghost loops that exist already at the one-loop level. Ghost loops nested within gluon loops do not produce particular effects, because the additional integrations over virtual momenta soften the IR divergence.

[4] Subleading terms are collectively taken into account by adding an extra constant in (18) the value of which is then determined by refitting the data (only for this parameter).

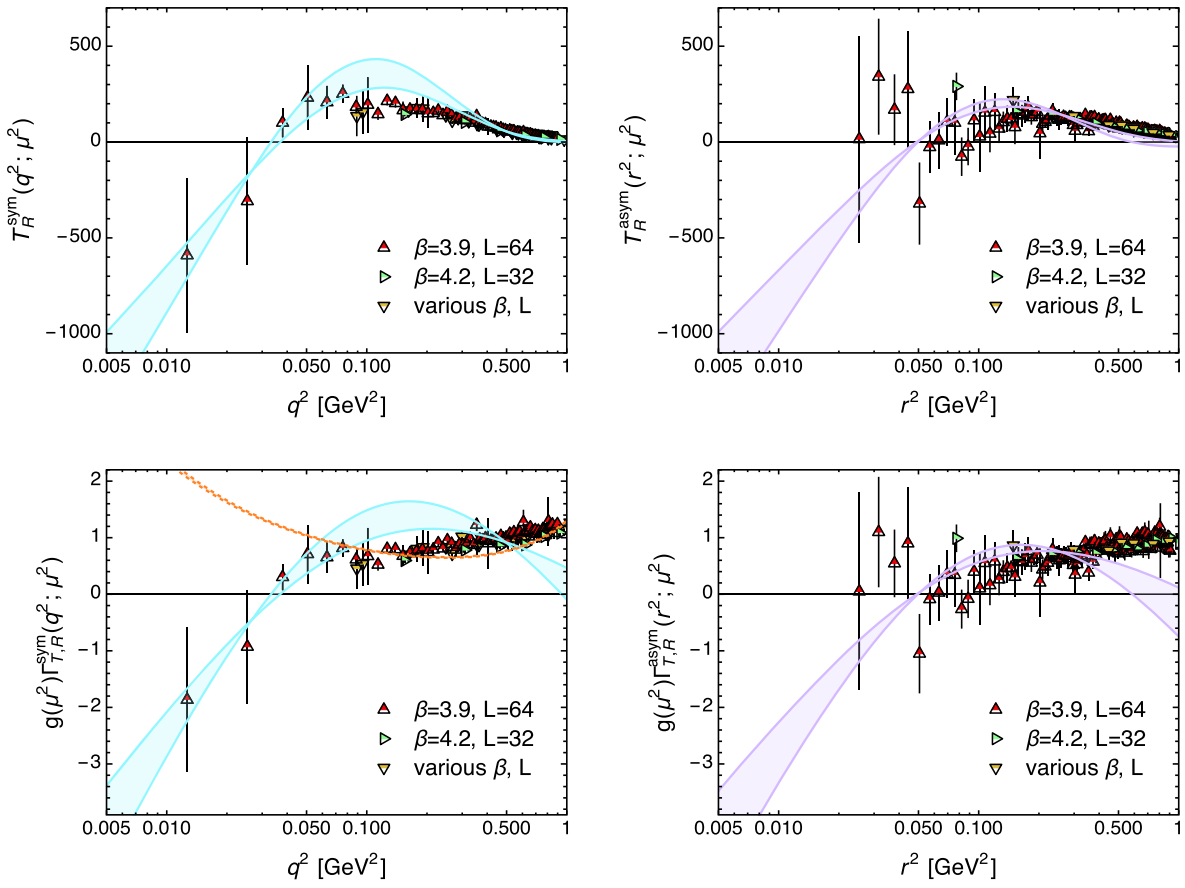


**Fig. 3.** (Color online.) Comparison between the lattice results for the renormalized connected and 1-PI form factors $T_R$ and $g\Gamma_{T,R}$ and the SDE prediction in the symmetric (left panels) and asymmetric (right panels) configurations. The band, as in Fig. 2, appears bounded by the results obtained with the fits of the lattice propagators for $L = 72$ and $L = 96$, and aims at giving an indication of the variation of the results. To ease the comparison, left and right panels have the same scale. Zero crossing happens at 190 and 220 MeV respectively. For the quantity $\Gamma_{T,R}^{sym}$ (lower left panel) we also plot (dashed line) the semiclassical approximation (19).

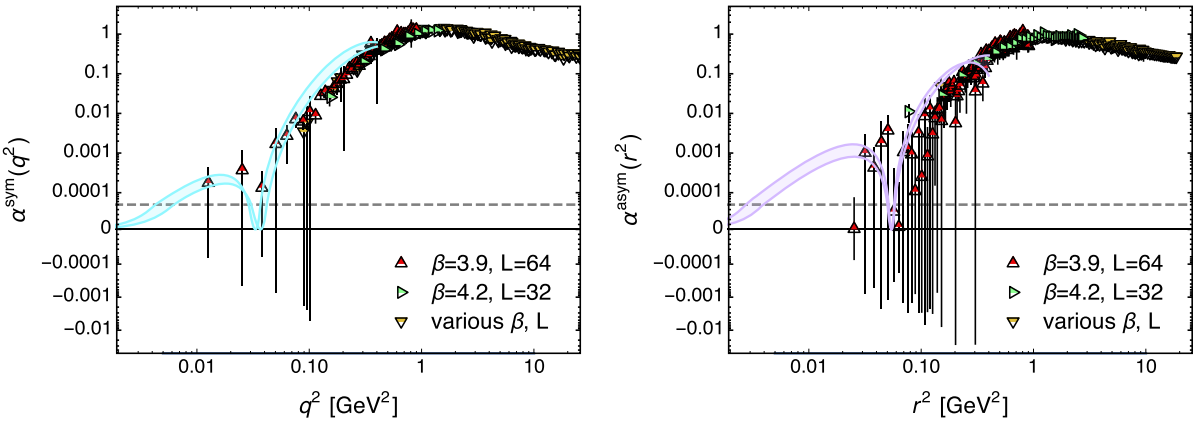


**Fig. 4.** (Color online.) Comparison between the lattice results for the three gluon effective coupling and the SDE prediction in the symmetric (left) and asymmetric (right) configuration. Notice that on the $y$ axis scale switch from logarithmic to linear at the location of the dashed gray line (and then back to logarithmic for $y < 0$); while this choice exaggerates the error bars, it has the advantage of exposing the vanishing of the coupling at a nonvanishing momentum value.

of $T$ was then scrutinized in detail and contrasted with (model-independent) SDE predictions finding good agreement. In doing so, we have discussed the failure of a semiclassical picture based on instantons, due to the quantum effects associated to massless ghost loops. It would be interesting to improve the statistics of the asymmetric configuration, in an attempt to discern the zero crossing, which is expected to appear on theoretical grounds, and has indeed been established in three-dimensional SU(2) simulations [1,2]. In addition, a cleaner look at the positive excess observed in the low momentum region of this configuration might help us disentangle contributions characteristic to a particular gluon mass generation mechanism, proposed recently in [61].

## Acknowledgements

The research of J.P. and J. R-Q is supported by the Spanish MINECO under grant FPA2014-53631-C2-1-P and FPA2014-53631-C2-2-P and SEV-2014-0398, and Generalitat Valenciana under

grant Prometeo II/2014/066. S. Z. acknowledges support by the Alexander von Humboldt Foundation. We thank K. Cichy, M. Creutz, O. Pène, O. Philipsen, M. Teper, J. Verbaarschot for fruitful discussions. Numerical computations have used resources of CINES and GENCI-IDRIS as well as resources at the IN2P3 computing facility in Lyon.

## References

[1] A. Cucchieri, A. Maas, T. Mendes, Phys. Rev. D 74 (2006) 014503.
[2] A. Cucchieri, A. Maas, T. Mendes, Phys. Rev. D 77 (2008) 094510.
[3] A. Cucchieri, T. Mendes, PoS LAT2007 (2007) 297.
[4] A. Cucchieri, T. Mendes, PoS QCD-TNT09 (2009) 026.
[5] I. Bogolubsky, E. Ilgenfritz, M. Muller-Preussker, A. Sternbeck, Phys. Lett. B 676 (2009) 69–73.
[6] O. Oliveira, P. Silva, PoS LAT2009 (2009) 226.
[7] A. Ayala, A. Bashir, D. Binosi, M. Cristoforetti, J. Rodriguez-Quintero, Phys. Rev. D 86 (2012) 074512.
[8] A.G. Duarte, O. Oliveira, P.J. Silva, arXiv:1605.00594 [hep-lat].
[9] A.C. Aguilar, D. Binosi, J. Papavassiliou, Phys. Rev. D 78 (2008) 025010.
[10] P. Boucaud, et al., J. High Energy Phys. 06 (2008) 099.
[11] C.S. Fischer, A. Maas, J.M. Pawlowski, Ann. Phys. 324 (2009) 2408.
[12] J. Rodriguez-Quintero, J. High Energy Phys. 1101 (2011) 105.
[13] M. Pennington, D. Wilson, Phys. Rev. D 84 (2011) 119901.
[14] P. Maris, C.D. Roberts, Int. J. Mod. Phys. E 12 (2003) 297–365.
[15] A.C. Aguilar, A.A. Natale, J. High Energy Phys. 08 (2004) 057.
[16] P. Boucaud, et al., arXiv:hep-ph/0507104.
[17] C.S. Fischer, J. Phys. G 32 (2006) R253–R291.
[18] K.-I. Kondo, Phys. Rev. D 74 (2006) 125003.
[19] D. Binosi, J. Papavassiliou, Phys. Rev. D 77 (2008) 061702.
[20] D. Binosi, J. Papavassiliou, J. High Energy Phys. 0811 (2008) 063.
[21] P. Boucaud, J.P. Leroy, A. Le Yaouanc, A.Y. Lokhov, J. Micheli, O. Pene, J. Rodriguez-Quintero, C. Roiesnel, J. High Energy Phys. 03 (2007) 076.
[22] D. Dudal, S.P. Sorella, N. Vandersickel, H. Verschelde, Phys. Rev. D 77 (2008) 071501.
[23] D. Dudal, J.A. Gracey, S.P. Sorella, N. Vandersickel, H. Verschelde, Phys. Rev. D 78 (2008) 065047.
[24] K.-I. Kondo, Phys. Rev. D 84 (2011) 061702.
[25] A.P. Szczepaniak, E.S. Swanson, Phys. Rev. D 65 (2002) 025012.
[26] A.P. Szczepaniak, Phys. Rev. D 69 (2004) 074031.
[27] D. Epple, H. Reinhardt, W. Schleifenbaum, A. Szczepaniak, Phys. Rev. D 77 (2008) 085007.
[28] A.P. Szczepaniak, H.H. Matevosyan, Phys. Rev. D 81 (2010) 094007.
[29] P. Watson, H. Reinhardt, Phys. Rev. D 82 (2010) 125010.
[30] P. Watson, H. Reinhardt, Phys. Rev. D 85 (2012) 025014.
[31] L. Chang, C.D. Roberts, Phys. Rev. Lett. 103 (2009) 081601.
[32] L. Chang, C.D. Roberts, P.C. Tandy, Chin. J. Phys. 49 (2011) 955–1004.
[33] S.-x. Qin, L. Chang, Y.-x. Liu, C.D. Roberts, D.J. Wilson, Phys. Rev. C 84 (2011) 042202.
[34] S.-x. Qin, L. Chang, Y.-x. Liu, C.D. Roberts, D.J. Wilson, Phys. Rev. C 85 (2012) 035202.
[35] A. Bashir, L. Chang, I.C. Cloet, B. El-Bennich, Y.-X. Liu, et al., Commun. Theor. Phys. 58 (2012) 79–134.
[36] G. Eichmann, Prog. Part. Nucl. Phys. 67 (2012) 234–238.
[37] I.C. Cloet, C.D. Roberts, Prog. Part. Nucl. Phys. 77 (2014) 1–69.
[38] D. Binosi, L. Chang, J. Papavassiliou, C.D. Roberts, Phys. Lett. B 742 (2015) 183–188.
[39] D. Binosi, J. Papavassiliou, Phys. Rep. 479 (2009) 1–152.
[40] J.M. Cornwall, Phys. Rev. D 26 (1982) 1453.
[41] M. Tissier, N. Wschebor, Phys. Rev. D 84 (2011) 045018.
[42] A.C. Aguilar, D. Binosi, D. Ibañez, J. Papavassiliou, Phys. Rev. D 89 (2014) 085008.
[43] M. Pelaez, M. Tissier, N. Wschebor, Phys. Rev. D 88 (2013) 125003.
[44] A. Blum, M.Q. Huber, M. Mitter, L. von Smekal, Phys. Rev. D 89 (2014) 061703.
[45] G. Eichmann, R. Williams, R. Alkofer, M. Vujinovic, Phys. Rev. D 89 (2014) 105014.
[46] A.K. Cyrol, L. Fister, M. Mitter, J.M. Pawlowski, N. Strodthoff, arXiv:1605.01856 [hep-ph].
[47] D. Binosi, D. Ibañez, J. Papavassiliou, J. High Energy Phys. 1409 (2014) 059.
[48] A.K. Cyrol, M.Q. Huber, L. von Smekal, Eur. Phys. J. C 75 (2015) 102.
[49] A.C. Aguilar, D. Binosi, J. Papavassiliou, Phys. Rev. D 86 (2012) 014032.
[50] A.C. Aguilar, D. Binosi, J. Papavassiliou, Phys. Rev. D 88 (2013) 074010.
[51] C.T. Figueiredo, A.C. Aguilar, http://sites.ifi.unicamp.br/qcd-tnt4/files/2015/08/figueiredo.pdf, 2015.
[52] R. Williams, C.S. Fischer, W. Heupel, Phys. Rev. D 93 (2016) 034026.
[53] J.S. Ball, T.-W. Chiu, Phys. Rev. D 22 (1980) 2550.
[54] B. Alles, D. Henty, H. Panagopoulos, C. Parrinello, C. Pittori, D.G. Richards, Nucl. Phys. B 502 (1997) 325–342.
[55] P. Boucaud, J.P. Leroy, J. Micheli, O. Pene, C. Roiesnel, J. High Energy Phys. 10 (1998) 017.
[56] A. Athenodorou, P. Boucaud, F. De Soto, J. Rodríguez-Quintero, S. Zafeiropoulos, arXiv:1604.08887 [hep-ph].
[57] P. Boucaud, F. De Soto, A. Le Yaouanc, J.P. Leroy, J. Micheli, H. Moutarde, O. Pene, J. Rodriguez-Quintero, J. High Energy Phys. 04 (2003) 005.
[58] P.J. Green, B.W. Silverman, Nonparametric Regression and Generalized Linear Models: A Roughness Penalty Approach, Monographs on Statistics & Applied Probability, vol. 58, Chapman & Hall, 1994.
[59] P.A. Grassi, T. Hurth, M. Steinhauser, Ann. Phys. 288 (2001) 197–248.
[60] D. Binosi, J. Papavassiliou, Phys. Rev. D 66 (2002) 025024.
[61] A.C. Aguilar, D. Binosi, C.T. Figueiredo, J. Papavassiliou, Phys. Rev. D 94 (2016) 045002.